The Bundle Dispersion of SWNT on Interaction with *p*-Terphenyl

Theresa G. Hedderman[1]*, *Anika S. Mostaert*[2], *Anne E. Shanahan*[1], *Hugh J. Byrne*[1]

[1]Focas Institute, Dublin Institute of Technology, Kevin Street, Dublin 8, Ireland.

[2]Conway Institute of Biomolecular and Biomedical Research, University College Dublin, Dublin 4, Ireland.

theresahedderman@dit.ie, Anika.Mostaert@ucd.ie, Anne.Shanahan@dit.ie, hugh.byrne@dit.ie .

RECEIVED DATE

CORRESPONDING AUTHOR FOOTNOTE. Theresa Hedderman, Focas Institute, Dublin Institute of Technology, Kevin Street, Dublin 8, Ireland. Ph: +353 (1) 402 7907, Fax: +353 (1) 402 7904. theresahedderman@dit.ie,

ABSTRACT. This paper investigates the interaction and bundle dispersion of single walled carbon nanotubes (SWNT) produced by arc discharge and by the high pressure decomposition of carbon monoxide, often referred to as the HiPco method, in the presence of the molecule *p*-terphenyl. The study will show that the extent of SWNT bundle dispersion and the degree of interaction with *p*-terphenyl is related to the level of purity of the SWNT sample. This study compares the bundle dispersion and interaction of SWNT with *p*-terphenyl in their as produced state and after purification. A number of spectroscopic and microscopic techniques are used to probe the SWNT and their interaction with *p*-terphenyl. A technique such as energy dispersive analysis by x-ray (EDAX) is used to give an elemental

analysis of the SWNT samples before and after purification. Fluorescence and atomic force microscopy are used as techniques to assess the degree of interaction and bundle dispersion of the SWNT.

KEYWORDS: Fluorescence, bundled single walled carbon nanotubes, isolated single walled carbon nanotubes, *p*-terphenyl, atomic force microscopy, high pressure decomposition of carbon monoxide, arc discharge, x-ray diffraction, energy dispersive analysis.

INTRODUCTION

Obtaining pure, mono-disperse single walled carbon nanotubes (SWNT) of specific structures in large quantities is problematic. There is currently no literature on a production or processing method which is capable of achieving such specifications. Although SWNT are largely insoluble in solvents such as toluene, when added to SWNT/toluene suspensions, the hydrocarbon *p*-terphenyl has shown potential in this context. The hydrocarbon was shown to solubilise, and disperse bundles of SWNT with strong evidence of selectivity.[1,2] Much literature has been published with regards to the interaction of SWNT with various organic molecules.[1-7] However, it is well understood and documented in the literature that different SWNT production methods result in samples containing SWNT of different bundle size, length and diameter as well as different degrees of purity.[8,9] The impurities range from the metal catalyst used in the production process to amorphous carbon structures. The research questions posed are, to what degree do experimental results differ when one SWNT sample is substituted for another and what components of the sample are responsible for the differences if any observed. This paper examines two samples of SWNT, one produced by arc discharge and the other produced by the HiPco (High pressure decomposition of carbon monoxide) method and investigates their interaction with *p*-terphenyl under similar conditions. The aim is to elucidate whether SWNT produced by different methods under similar experimental condition exhibit similar or varying behaviour and if so the factors responsible for any variations observed. Such a study will yield a better understanding of SWNT processing techniques.

EXPERIMENTAL SECTION

Solutions in the range of ~4.5 x 10^{-12} to ~2.5 x 10^{-3} M for *p*-terphenyl in toluene were prepared. HiPco SWNT (H-SWNT) obtained from Carbon Nanotechnologies Incorporated (CNI) (http://www.cnanotech.com)[9] and arc discharge SWNT (AD-SWNT) obtained from Montpellier University (now, http://www.nanoledge.com)[10,11,12] were added to all *p*-terphenyl solutions in a 1:1 weight ratio (w/w); of SWNT/*p*-terphenyl. Both the composite solutions and solutions containing *p*-terphenyl were sonicated using an ultra sonic tip (ultrasonic processor VCX, 750 Watts) for 30s and allowed to settle for 24 hours after which the supernatant liquid from the composite solutions was carefully withdrawn. The composite solutions were then allowed to settle for a further 24 hours before characterization. The precipitate of the composite solutions was found to be relatively rich in SWNT so solubility of the SWNT is only partial. Concentrations are quoted as prepared. Analytical techniques employed in this paper are, UV/Vis/NIR absorption spectroscopy (Perkin Elmer Lambda 900), fluorescence spectroscopy (Perkin Elmer LS55), Raman spectroscopy (JobinYvon, Instruments SA LabRam 1B with a confocal Raman imaging microscope), atomic force microscopy (AFM) (Asylum MFP-3D) and energy dispersive analysis by x-ray EDAX (Jeol 8600).

The samples of SWNT were purified following the procedure given below. This procedure was adapted from Cheng *et al.*[13] A mass of 25 mg of Hipco and 20 mg of arc discharge SWNT were washed with de-ionised water followed by the addition of 37 % HCL and sonication for two minutes with the sonic tip (ultrasonic processor VCX, 750 Watts) at forty percent power to allow iron catalyst dissolution. The samples were left to stir overnight. The following day the samples were filtered and washed with copious amounts of de-ionised and allowed to dry.

The UV-Vis-NIR spectrometer used to probe the materials in this paper was the Perkin Elmer Lambda 900 spectrometer. The spectrometer is a double-beam, double monochromator ratio recording system with pre-aligned tungsten-halogen and deuterium lamps as sources. The wavelength range is from 175 to 3,300 nm with an accuracy of 0.08 nm in the UV-Vis region and 0.3 nm in the NIR region. It has a photometric range of ± 6 in absorbance. For all of the experimental studies, the absorption was measured at all times with a reference sample in a double beam arrangement; the purpose being to

eliminate variations caused by the difference in lamp intensities at different frequencies. Samples were prepared by dropcasting SWNT samples onto the quartz cell and allowing them to dry before characterization.

The Perkin Elmer LS55 luminescence spectrometer was computer controlled. Excitation is provided by a pulsed Xenon discharge lamp with a pulse width at half peak height of < 10 μs and pulse power 20 kW. The source is monochromated using a Monk-Gillieson type monochromator and can be scanned over the range of 200-800 nm. The luminescence is passed through a similar monochromator, which can be scanned over the range of 200-900 nm. For analysis of samples a 10ml quartz cuvette was filled with the appropriate solutions.

The Raman instrument used was the Instruments SA LabRam 1B with a confocal Raman imaging microscope system. Both Helium-Neon (632.8 nm/11 mW) and Argon ion (514.5 nm/130 mW, 488 nm/130 mW, 457 nm/20 mW) were available as sources. The light is imaged to a diffraction limited spot (typically 1 μm) via the objective of an Olympus BX40 microscope. For Raman imaging the samples were dropcast onto a glass slide and allowed to dry overnight before analysis.

The EDAX instrument is a Jeol 8600 microprobe. The microprobe consists of an electron gun and a system of electromagnetic lenses for producing a beam and scanning coils to allow the beam to be rastered across the specimen. The intensity of the x-rays is a measure of the proportions of the elements present. Quantitative analysis using wavelength dispersive spectrometry requires both a stable, well tuned instrument and standards for comparison that are both well characterised and appropriate to the given specimen. Quantitative analysis can address all elements heavier the lithium. For sample analysis powdered SWNT samples are scattered onto the sample disc which is coated in silver chloride.

The AFM used in this research was the Asylum MFP 3D (Asylum Research, Santa Barbara, http://www.asylumresearch.com/Products/Mfp3DIO/Mfp3DIO.shtml). The MFP-3D base and scanner have three configurations for illuminating and viewing the sample. The MFP-3D head has a sensored optical lever with diffraction limited optics and a low coherence light source virtually eliminates interference artifacts. The sensored z axis provides precise measurements of the cantilever position for

accurate force and topography measurements. AFM imaging was conducted in air and was performed in intermittent-contact mode using Si_3Ni_4 cantilevers (CSC36 series, MikroMasch) with a spring constant of approximately 5 N/m. Igor pro (Wavemetrics, OR) software was used to analyse the image data. For AFM studies the composite samples were dispersed on an activated silicon surface and this involved covering the silicon surface in a layer of 3-aminopropyl tri-ethoxysilane (APTES) for 10 minutes followed by a rinse with de-ionised water and then drying at room temperature. The activated surface was then immersed in the composite solution for approximately three weeks and once removed from the solution the surface was rinsed with de-ionised water and allowed to dry at room temperature before imaging.

RESULTS AND DISCUSSION

For the study presented in this paper the hydrocarbon *p*-terphenyl was chosen because it has been previously shown to interact with, suspend and disperse bundles SWNT in organic solvents.[1,2] The solvent toluene was chosen because it is a non polar solvent and therefore a high degree of solubility of *p*-terphenyl is exhibited as both components are non polar. The solvent toluene also exhibits a poor affinity for the retention of SWNT and therefore solubilisation of the SWNT *via* an interaction with *p*-terphenyl can be easily monitored.[1,2,14] Two samples of SWNT were investigated, arc discharge SWNT (AD-SWNT) and HiPco SWNT (H-SWNT). The arc-discharge method in principle is based on an electric arc generated between two graphite electrodes under an inert atmosphere of helium or argon. Two graphite rods are used as electrodes. A current is passed through the electrodes and plasma is created between them. The temperature in the plasma region is ~ 4000 K and the carbon is sublimated and the positive electrode which contains the catalysts Y/Ni/C 1 %/ 4%/ 95% is consumed. The method produces SWNT of a broad diameter range with an average diameter of 1.4 nm as well as amorphous carbon, spherical metallic nanoparticles, fullerenes and graphitic sheets The sample purity was estimated at 70 % and the bundle size at approximately 20 tubes per bundle.[10] In the Hipco process the tubes are produced by a gas phase catalytic process. The catalyst particles for SWNT growth form in

situ as a result of the thermal decomposition of iron pentacarbonyl, with a heated flow of carbon monoxide at pressures of 1-10 atm and temperatures of 1100 – 1500 K. A sample purity of ~90 % SWNT is estimated and in contrast to the arc method the HiPco method produces SWNT of a narrow diameter range with the average diameter of 1.1 nm. The bundles produced are reported to contain on average 20 to 40 tubes.[9] The main impurity in the HiPco sample is approximately 10 wt% iron catalyst particles which are encased in thin carbon shells and distributed throughout the sample as 3-5 nm particles.

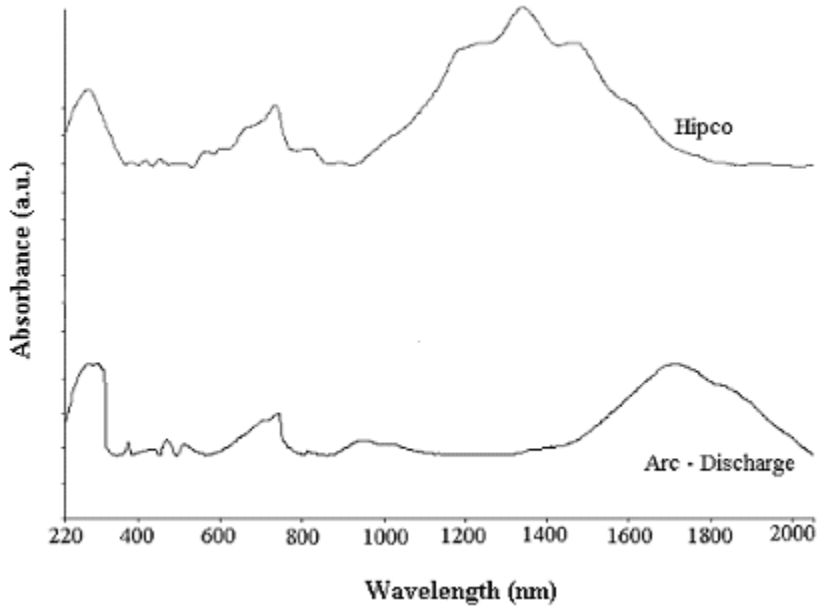

Figure 1. UV-Vis-NIR absorbance spectra of arc-discharge and HiPco SWNT.

To demonstrate the different diameter distributions of SWNT within each sample UV/vis/NIR absorbance spectra of both the Hipco (H-SWNT) and arc-discharge SWNTs (AD-SWNT) were taken and are depicted in Figure 1. The features observed have origin in the singularities in the diameter dependent density of states (DOS).[15] It is immediately obvious that the absorption spectra of both SWNT samples differ. Therefore it may be concluded that the UV-Vis-NIR spectral profiles of SWNTs

are to a degree dependent on the production process. However the literature reports that the absorbance profile may also differ from batch to batch for SWNTs produced by the same process.[16-19] It may be deduced that the only information that can be taken from the UV-Vis-NIR spectra is the range of diameters of SWNTs present in that sample and the ratio of metallic to semi conducting SWNTs.

Theoretical predictions suggest that the absorbance bands of SWNTs can be ascribed to the inter-band transitions between the mirror image spikes in the density of stated (DOS) of SWNTs.[20] From electronic band theory, absorbances between 1400 – 1900 nm are assigned to the first inter-band transition v1 → c1 in semi conducting SWNTs , whereas the bands between 800 – 1100 nm are assigned to the second inter-band transitions v2 → c2 again in semi conducting SWNTs.[20] The predicted absorbance at 650 nm is believed to be the v1 → c1 of metallic SWNTs and weak bands at 550 nm and 300 nm are due to v3 → c3 in semi conducting SWNTs and v2 → c2 in metallic tubes respectively.[21] The absorbance at 270 nm is the π plasmon frequency of carbon material such as C_{60}, SWNTs, and graphite. The precise position of the SWNT absorption bands has been shown to be roughly described by the following equations;

$$E^{S}_{11} = 2k/d \qquad \text{Equation 1}$$

$$E^{S}_{22} = 4k/d \qquad \text{Equation 2}$$

$$E^{M}_{11} = 6k/d \qquad \text{Equation 3}$$

where k is a constant, d is the diameter, E is the energy transition and the superscripts S and M represent semiconducting and metallic SWNTs respectively whereas the subscripts 11 and 22 represent the first and second electronic transition between mirror spikes in the DOS.[22] However it has since been shown experimentally that the relationship between E^{S} and d is more complex than originally thought as

described by more current calculations by Bachilo *et al*.(2002).[21,23] The width of the van Hove bands are determined by the overlapping transitions from all different diameters and chiral indices.

Comparing the spectra in Figure 1, it is evident that AD–SWNT has a strong absorbance centered at ~1700 nm and ~950 nm which corresponds to the first and second inter-band transitions for semi conducting SWNTs. H–SWNT has absorbance centered at ~1400 and ~800 nm which also fall under the first and second inter-band transitions for semi conducting SWNTs. The fact that H–SWNT are centered at ~1400 nm compared to ~1700 nm indicates a different diameter distribution for the H–SWNT sample compared with AD–SWNT samples in that range. AD–SWNT and H–SWNT have a strong absorbance at ~650 nm and absorbance in this region corresponds to the first inter-band transition for metallic SWNTs. Absorbance at ~550 nm corresponds to the third inter-band transition for semi conducting SWNTs and it is evident in both the AD–SWNT and H-SWNT samples. Finally, the π plasmon band at ~270 nm is present in both SWNT samples. It is of interest to note that the H–SWNT spectrum exhibits more structure in this region compared to AD-SWNT and this is believed to be due to a smaller average tube diameter of about 1.1 nm resulting in a higher degree of structural information.[18,19,24]

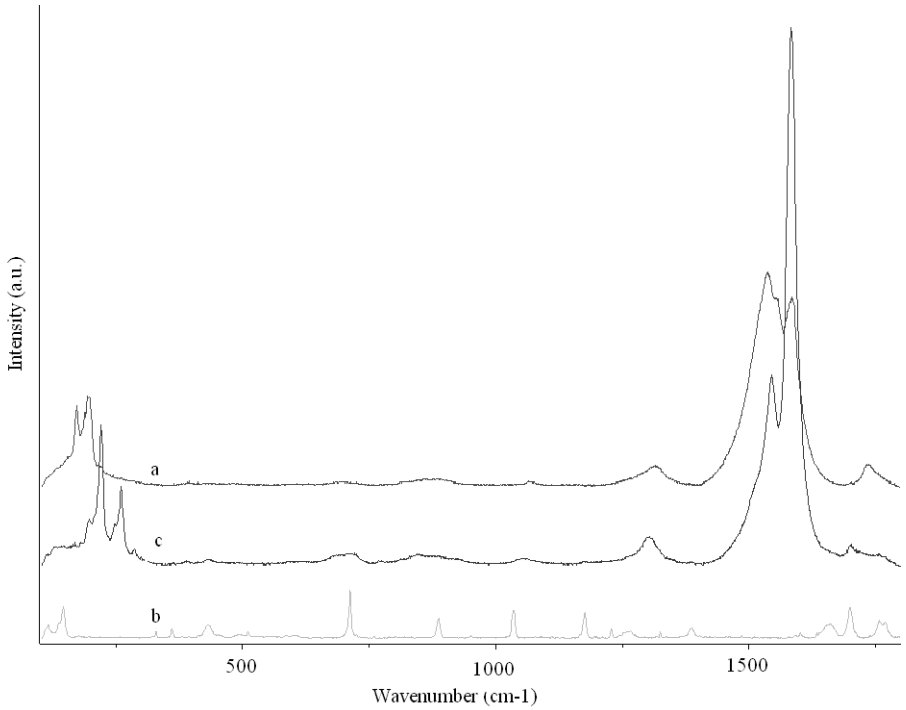

Figure 2. Raman spectra of (a) the untreated AD-SWNT, (b) the pristine p-terphenyl powder and (c) the composite sample at 2.5 x 10-3 M a 1:1 w/w ratio of p-terphenyl/SWNT at laser excitation 632.8 nm.

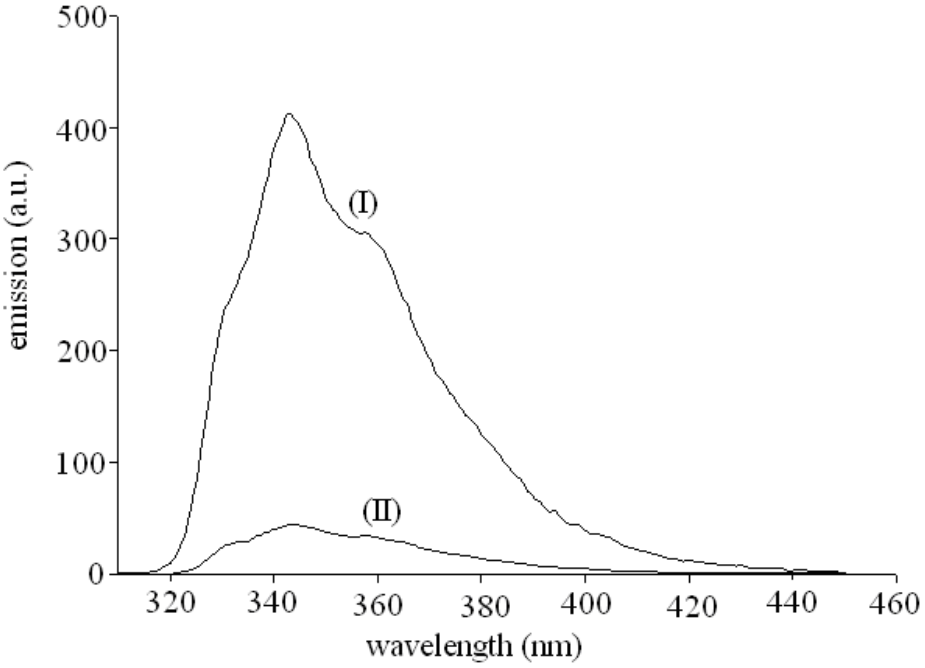

Figure 3. The spectra represents the fluorescence of *p*-terphenyl at excitation wavelength of 300 nm in the absence (I) and presence (II) AD-SWNT at a concentration of 2.5 x 10^{-3} M in toluene.

Figure 2 shows the Raman spectra of SWNT, p-terphenyl and the composite spectrum. The vibrational modes in SWNT consist of optical and acustic modes, such as of out-of–plane, in-plane and in-plane radial modes. Three phonon modes dominate the Raman spectrum of SWNTs. In the low frequency region, the phonon modes are dominated by the radial out-of-plane modes whose frequency is diameter-related often referred to as the radial breathing modes (RBMs). In the medium frequency region, both radial and tangential modes (stretching and bending modes) are present, and the detailed structure of the spectrum depends not only on the diameter but also on the helicity. In the high frequency region, the phonon modes are dominated by the tangential modes (G-line). Figure 2 depicts the Raman spectrum for an as produced sample of untreated AD-SWNT with an excitation wavelength

of 632.8 nm. Although theory predicts that SWNTs have 15 or 16 Raman allowed vibrational modes, experimental evidence shows only a few intense and several weaker modes.25,26 The intensity of the Raman modes not only depends on parameters such as the SWNT process method and the geometry of the SWNT but also on the bundle thickness.27 With respect to p-terphenyl in Figure 2 the modes at 1603 cm-1 and 1592 cm-1 may be attributed to the C=C stretches in p-terphenyl with the vibrational mode at 1271 cm-1 representing a ring stretch. The vibrational modes at 1003 cm-1 and 988 cm-1 are due to ring breathing modes and at 770 cm-1 a ring vibrational mode is observed. The spectra in Figures 2 (a) and (b) agree well with those reported in the literature.28

Comparing Figure 2 (a) with Figure 2(c) the characteristic features of the SWNT spectrum have been changed in composite spectrum (Figure 2(c)) in comparison to that of the pristine SWNT sample (Figure 2(a)). The spectral changes are not simply due to the addition of the *p*-terphenyl whose spectrum is shown in Figure 2(b). Notably the changes to the distribution of the RBM's which are diameter dependent is an indication of a change in the local environment of the SWNTs and also indicative of bundle dispersion. Similar results were observed in the case of H-SWNT and *p*-terphenyl solutions at similar concentrations.

In fluorescence spectroscopy molecules that absorb photons can discard its excess energy *via* radiative decay, in which an electron relaxes back into the lower energy levels of the ground electronic state and in the process generates a photon and yields information with regards to the electronic and vibrational levels of the ground electronic state. The two materials used in this study undergo fluorescent radiative decay. However only *p*-terphenyl is discussed as the fluorescence of the SWNTs was beyond the range of the fluorimeter used.[29] Figure 3 shows the fluorescence of *p*-terphenyl before and after the addition of AD-SWNT.

p-Terphenyl is known to have an emission maximum at 345 nm, as shown in Figure 3(I). Upon addition of SWNT to *p*-terphenyl/toluene solutions, the fluorescence is visibly seen to quench Figure 3(II). This quenching is an indication that an interaction occurs between the *p*-terphenyl molecules and the SWNTs as the fluorescence energy of *p*-terphenyl is lost in the π stacking between the two

components.[1] To gain a better understanding of the results obtained in Figure 3, the behaviour of *p*-terphenyl and its interaction with SWNT, the fluorescence of *p*-terphenyl over a broad range of concentrations in toluene were probed.

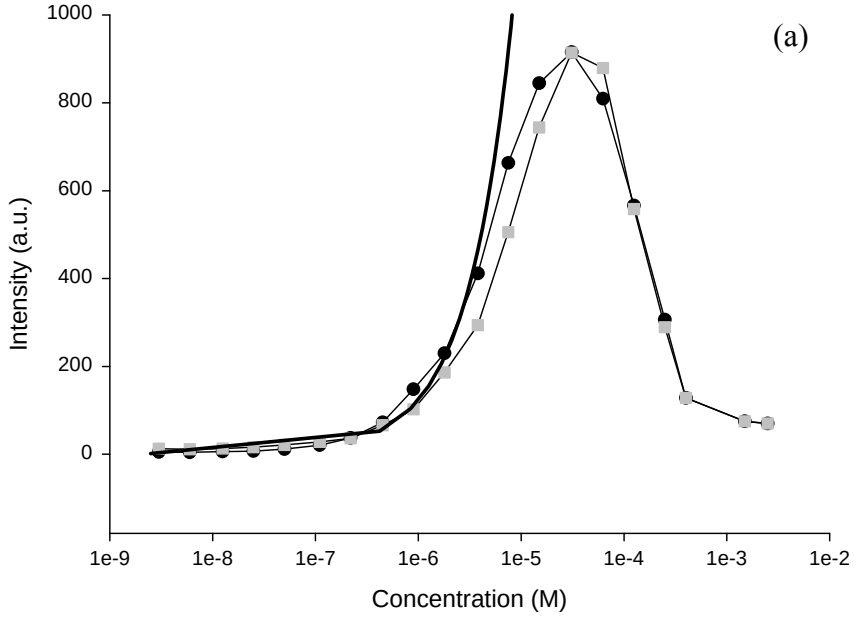

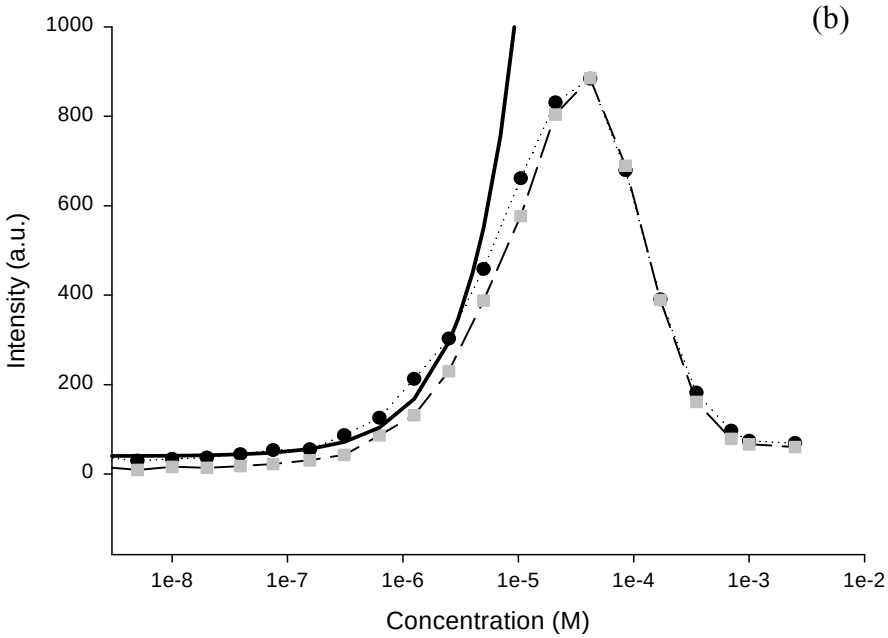

Figure 4. Fluorescence of *p*-terphenyl at an excitation wavelength of 300 nm within a concentrations range of ~2.5 x 10^{-9} and ~2.5 x 10^{-3} M in the absence (filled black circles) and presence (filled grey squares) of SWNT at a 1:1 w/w ratio on a linear/log axis. The solid line denotes a linear fit. The filled grey squares in (a) represent the presence of AD-SWNT and (b) H-SWNT both at a 1:1 w/w ratio with respect to *p*-terphenyl.

Two sets of samples were prepared, one set contained just *p*-terphenyl and the second set contained similar concentrations of the *p*-terphenyl/SWNT at a 1:1 w/w ratio. The fluorescence of the *p*-terphenyl in the absence and presence of SWNT yields information with regards to the interaction between the two components. Changes in the aggregation process of *p*-terphenyl are monitored on the addition of SWNT.

The fluorescence of *p*-terphenyl in the absence (filled black circles) and presence of AD-SWNT (filled grey squares) is depicted in Figure 4 (a) within the concentration range of ~2.5 x 10^{-9} and ~2.5 x 10^{-3} M. With respect to *p*-terphenyl (filled black circles) the concentration dependence of the fluorescence fits well to a linear increase between ~2.5 x 10^{-9} and ~4 x 10^{-6} M denoted by the black solid line (note the plot is depicted in a linear/log axes format). Within a concentration range of ~4 x 10^{-6} to ~2.5 x 10^{-3} M the fluorescence of *p*-terphenyl deviates from linearity and this deviation is evident both at the spectral maximum and on the red side of the spectrum, indicating that it is not due to re-absorption. Therefore the deviation is attributed to the formation of aggregates of *p*-terphenyl which causes quenching of the fluorescence.

Upon the addition of AD-SWNT (filled grey squares) to the *p*-terphenyl solutions at a 1:1 w/w ratio, the composite fluorescence trend appears similar to that of the *p*-terphenyl discussed in the previous paragraph but with quenching evident due to interaction with the SWNT, within the concentration range of ~2.5 x 10^{-9} and ~2 x 10^{-5} M. Between a concentration of ~4 x 10^{-5} M and 1 x 10^{-4} M the composite fluorescence deviates from linearity and relative to the fluorescence of *p*-terphenyl the composite

fluorescence is now in excess. The additional fluorescent intensity observed is explained by the dispersion of the *p*-terphenyl aggregates as the fluorescence data suggests that the presence of SWNT interferes with and hinders the aggregation process of *p*-terphenyl. This affect on aggregation indicates that *p*-terphenyl preferentially interacts with the SWNT and suggests that the binding energy of *p*-terphenyl/SWNT is greater than the binding energy between *p*-terphenyl/*p*-terphenyl. This suggestion is not unreasonable since theoretical binding energy calculations and thermal desorption studies show that polycyclic aromatic hydrocarbons and graphite (PAH/graphite) interactions are more favourable than the PAH/PAH interactions.[30-33] Similar results were observed in the case where H-SWNT replaced AD-SWNT and the results are depicted in Figure 4 (b). The only significant difference between Figure 4 (a) and (b) is that at ~1 x 10^{-4} M the excess fluorescence is more evident in Figure 4 (a) perhaps indicating that AD-SWNT interact with and more effectively disperse *p*-terphenyl molecules. The hydrocarbon *p*-terphenyl and SWNT are non polar molecules. Non polar molecules interact *via* van der Waals forces, also known as dispersion forces. Dispersion forces can be exhibited by non polar molecules because electron density moves about the molecules probabilistically. When electrons are more concentrated in part of the molecule a temporary multipole is created. Dispersion forces become stronger as the molecule becomes bigger hence the preferred interaction between the hydrocarbons with SWNT as opposed to itself. The AD-SWNT contains SWNT of larger diameters compared with the Hipco sample and perhaps for this reason AD-SWNT interacts more strongly with and are more effective at dispersing *p*-terphenyl aggregates compared with H-SWNT.

To conclude, the study in Figure 4 indicates the concentration range where *p*-terphenyl exists as isolated and aggregated molecules and that the presence of SWNT hinders the aggregation of *p*-terphenyl molecules and this is expressed by the excess emission of *p*-terphenyl in the composite solutions compared to the fluorescence of *p*-terphenyl alone.

To follow on from the study in Figure 4 further fluorescence studies were conducted to probe the extent of bundle dispersion of the SWNT in the presence of *p*-terphenyl in toluene with decreasing concentration. The model to investigate the bundle dispersion of SWNT is described in references 1 and

5 and the model is adapted to this study to monitor and compare the extent of bundle dispersion of both the H-SWNT and AD-SWNT. The model is based on the concentration dependent interaction of organic molecules with SWNT at a 1:1 w/w ratio of SWNT/organic molecules. [1,5] Thus all concentrations quoted refer to 1:1 ratios by mass, w/w of *p*-terphenyl and are quoted in terms of *p*-terphenyl concentration. The model presented is for low concentrations and when the system is in equilibrium the adsorption rate equals the desorption rate.[5] The adsorption rate was calculated theoretically; representing a SWNT (or bundle) as a cylinder and assuming that any molecule that reaches the SWNT adsorbs via van der Waals interactions. The desorption rate was shown to follow first order kinetics and was calculated as a function of the number of bound molecules per unit volume, the volume of solution occupied by one SWNT. As the fraction of free fluorescent molecules changes over the concentration range studied, a relationship is derived whereby the change in the fraction of free fluorescent molecules could be described by a characteristic concentration C_0 and SWNT concentration $C_{NT.}$

Equation 4 represents the equilibrium at which the adsorption rate equals the desorption rate, where N_F is the number of free molecules, N_B is the number of bound molecules, Fl_{comp} is the fluorescence of the composite and Fl_{mol} is the fluorescence of the fluorescent organic molecule which gives the fraction of free fluorescent organic molecules in solution. The model is derived for 1:1 w/w ratios and so for all concentrations the partial SWNT concentration, C_{NT}, equals the partial molecular concentration, C_m.

$$N_F / (N_F + N_B) = 1 / (1 + C_{NT} / C_0) = Fl_{comp} / Fl_{mol} \qquad \text{Equation 4}$$

C_0 is an important term as it contains much of the information about the dynamics of the system (Equations 4 and 5).[1,5] The binding energy of the p-terphenyl with the SWNTs is described by E_B and the SWNT bundle surface area by A_{bun}. The C_0 value is sensitive to such things as the viscosity of the solvent and the size of the hydrocarbon and these are both accounted for in the diffusion (*D*) term. The varying SWNT bundle mass (ρ_{bun}) and surface area A_{bun} are recognised as factors that will effect the

position of the C_0 curve which is also dependent on the binding energy E_B. Other parameters within the equation are υ which represents a pre-exponential factor and describes desorption of organic molecules from graphitic surfaces whereas *f*, the space integral, describes the probability of the organic molecule reaching the SWNT bundle and adsorbing to it.

$$C_0 = \pi^2 \upsilon \rho_{bun} A_{bun} e^{-E_B/kT}/(48Df) \qquad \text{Equation 5}$$

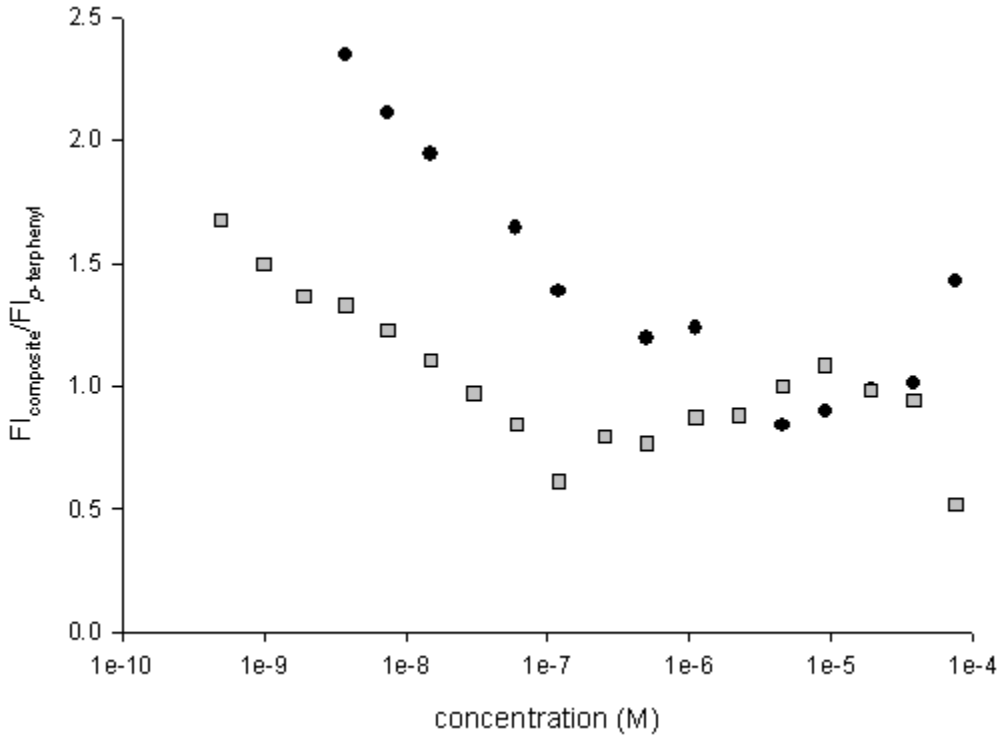

Figure 5. A plot of the fraction of free *p*-terphenyl on interaction with H-SWNT (blackcircles) and AD-SWNT (grey squares) in their as produced state (defined by Fl_{comp}/Fl_{mol}), as a function of concentration of *p*-terphenyl.

Adapting the model to the fluorescence studies above and applying Equation 4 to Figure 5, a plot of the fraction of free *p*-terphenyl on interaction with SWNT as a function of concentration of *p*-terphenyl

where SWNT are present at a 1:1 w/w ratio is achieved as a result of the interaction between the two components.

Figure 5 is a plot of the fraction of free *p*-terphenyl on interaction with SWNT in their as produced state. What is interesting with this graph is that in the case of the H-SWNT and AD-SWNT the fluorescence of *p*-terphenyl exceeds 1.0 between a concentration range of 5 x 10^{-10} M to 4 x 10^{-8} M for AD-SWNT and 5 x 10^{-10} M to 5 x 10^{-6} M for H-SWNT respectively. This is within the range where isolated *p*-terphenyl occurs (see Figure 4).[1]Therefore the excess fluorescence could not be attributed to the destacking of *p*-terphenyl aggregates. The results raised the question as to whether or not impurities were present in the composite samples and if so were they responsible for the results observed. The AFM image in Figure 6 shows the presence of SWNT and impurities are evident within the composite sample.

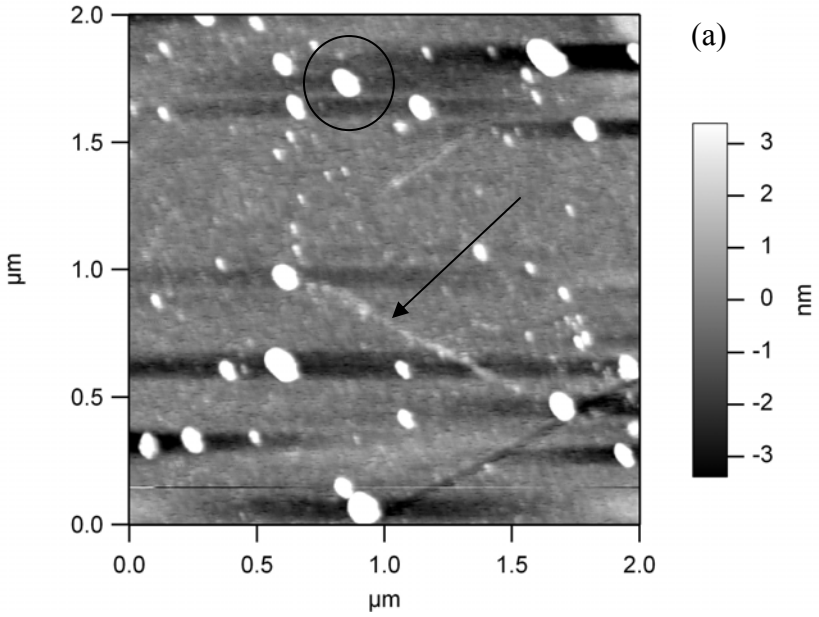

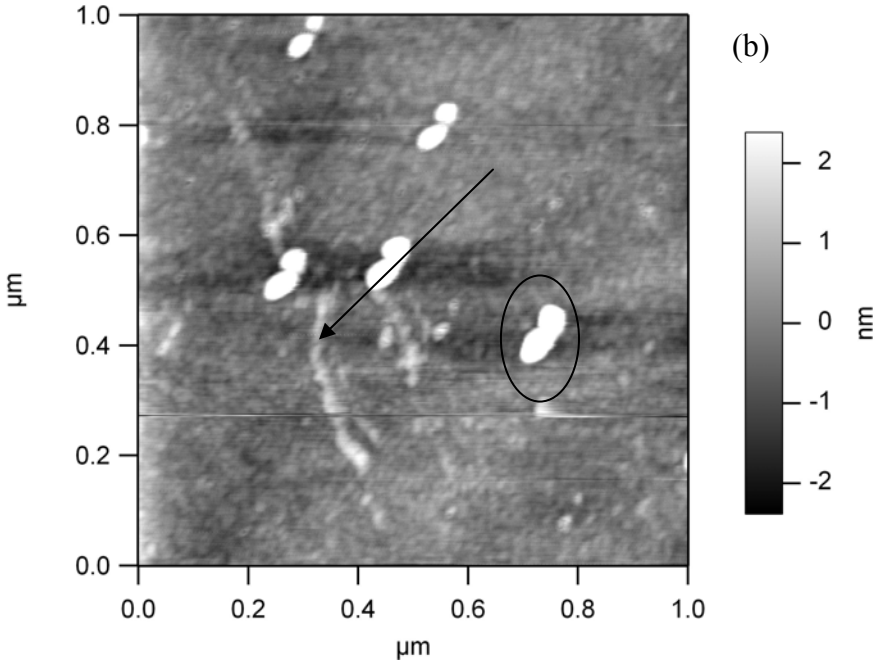

Figure 6. AFM of (a) AD-SWNT at ~1 x 10^{-8} M and (b) H-SWNT at ~1 x 10^{-8} M for *p*-terphenyl with SWNT present at a 1:1 w/w ratio of *p*-terphenyl/SWNT. The arrows point to the SWNT in the composite samples and the impurities are circled by the black ring.

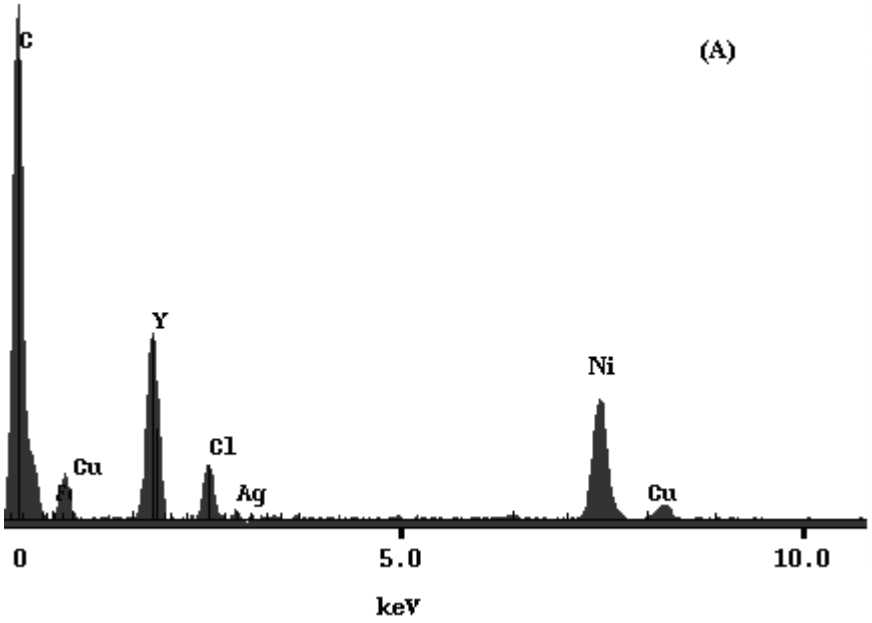

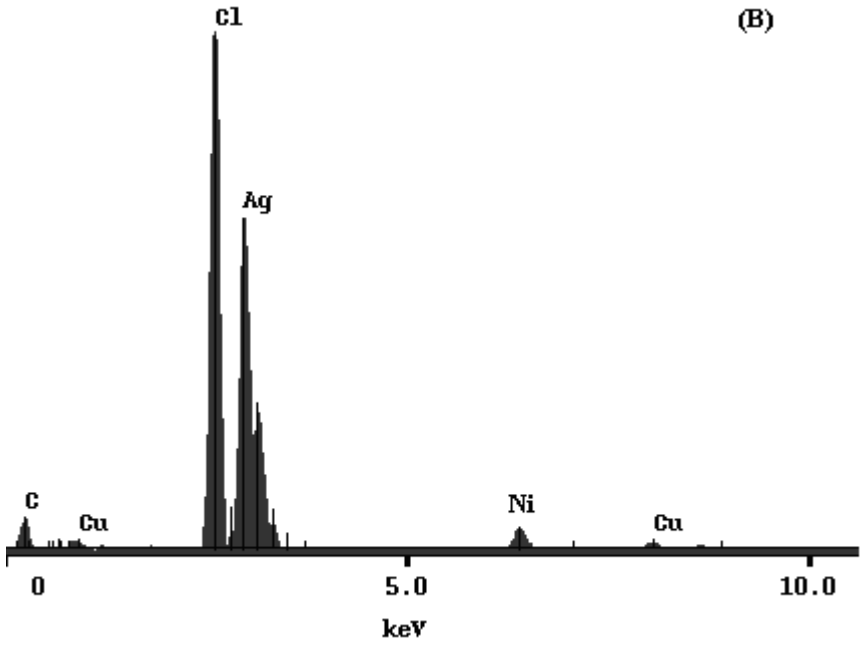

Figure 7. Energy Dispersive Analysis by X-ray (EDAX) was conducted on AD-SWNT before (A) and after (B) purification.

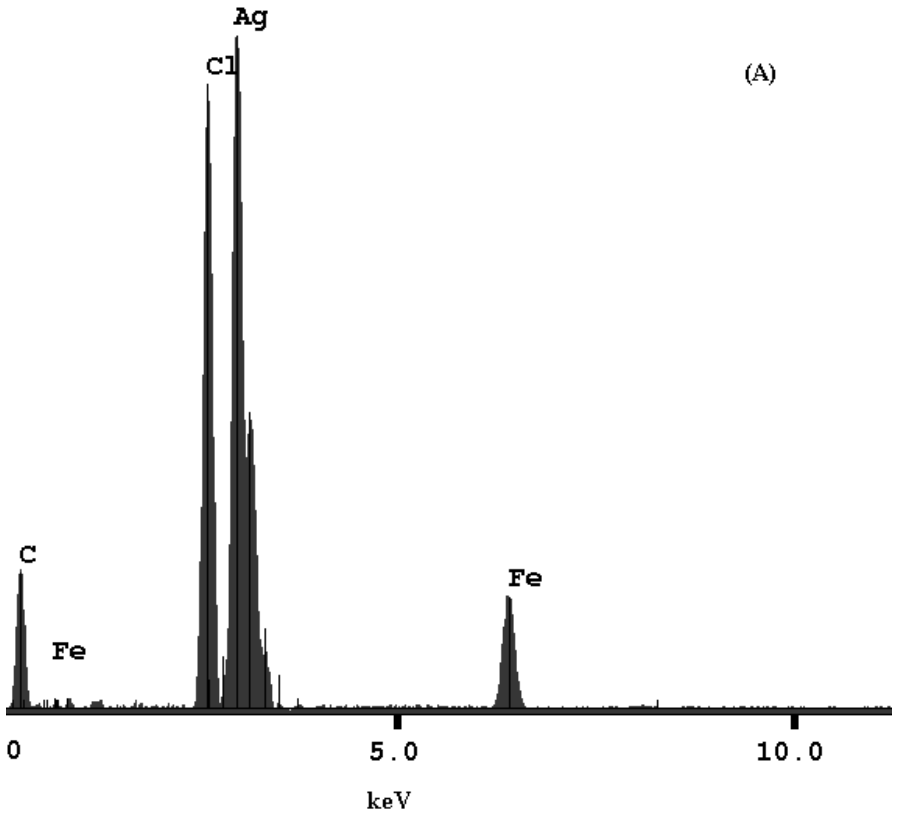

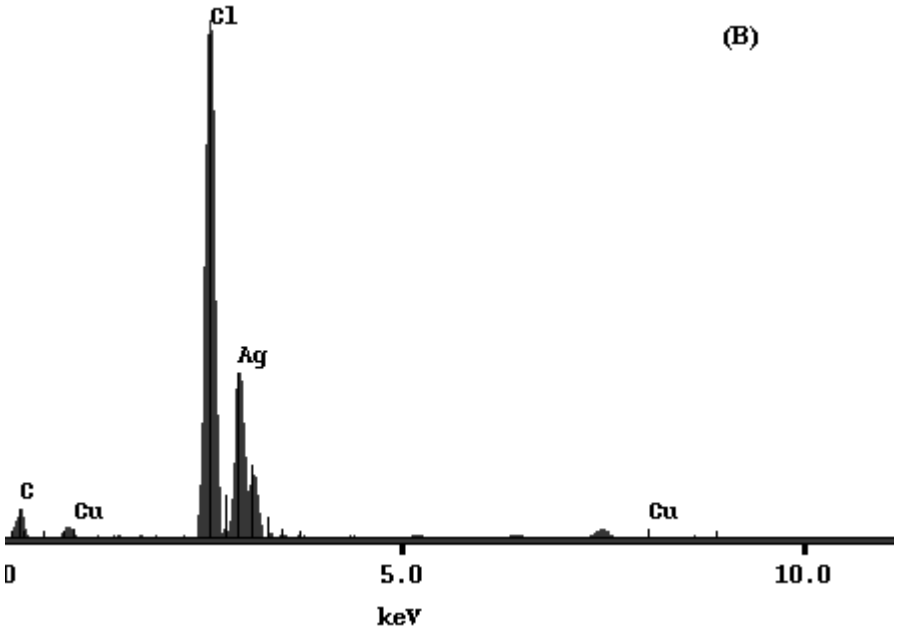

Figure 8. Energy Dispersive Analysis by X-ray (EDAX) was conducted on H-SWNT before (A) and after (B) purification.

The as produced samples of AD-SWNT and H-SWNT were purified as described in the experimental section. Energy dispersive analysis by X-ray (EDAX) was conducted on the SWNT samples before and after the purification process to assess the degree of success of the method and the results presented in Figures 7 and 8. In Figure 7(A) the following elements are listed; C for carbon, Cu for copper, Y for yttrium, Cl for chlorine, Ag for silver and Ni for nickel. The carbon, yttrium and nickel are all components of the as produced AD-SWNT sample. The chlorine and silver are components of the paint used to retain the SWNT sample on the sample holder which comprises of copper, also seen in the analysis. Comparing Figure 7(B) the purified AD-SWNT sample with Figure 7(A), the as produced SWNT sample the yttrium peak is not observed in Figure 7(B) and both the nickel and carbon peaks are greatly reduced. This indicates that on purification the metal catalyst impurities are significantly reduced. The reduction in the carbon peak may be indicative of the removal of amorphous carbon from the sample. Similar results were observed for Figure 8. In Figure 8(A) the elements observed are carbon (C), iron (Fe) and the components of the paint chlorine and silver (Cl and Ag) for the as produced H-

SWNT sample. In Figure 8(B) the iron peak is no longer observed and the carbon peak is reduced when compared to Figure 8(A) indicating that purification of the SWNT sample was successful.

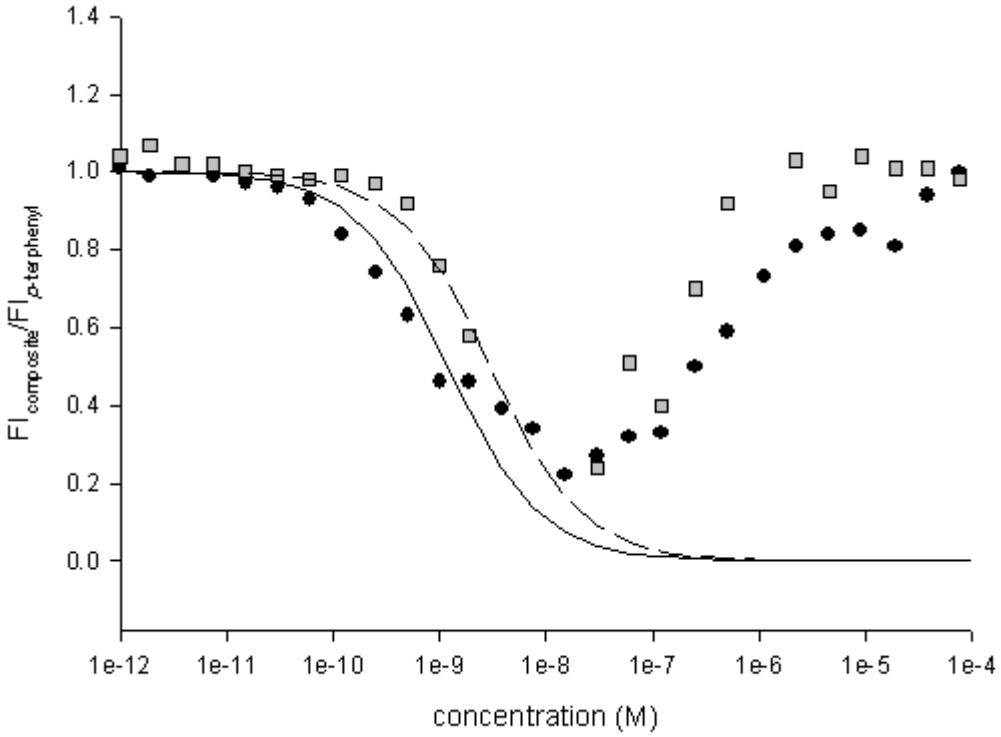

Figure 9. A plot of the fraction of free *p*-terphenyl on interaction with purified H-SWNT and AD-SWNT (defined by Fl $_{p\text{-terphenyl in the composite}}$/Fl $_{p\text{-terphenyl}}$), as a function of concentration of *p*-terphenyl. The solid line and the broken line are fits to Equation 1 for H-SWNT and AD-SWNT respectively. The black lines give a C_0 value of ~1.2 x 10^{-9} M and 4.2 x 10^{-9} M for H-SWNT and AD-SWNT respectively as a result of the interaction of *p*-terphenyl at a 1:1 w/w ratio.

The fluorescence study conducted in Figure 5 was repeated on the purified samples and the results are presented in Figure 9. Proceeding from left to right across Figure 9, from approximately ~1 x 10^{-11} to ~4x 10^{-8} M of *p*-terphenyl the fluorescence of the fraction of free *p*-terphenyl decreases steadily with increasing concentration. In this region, the free, isolated hydrocarbon and SWNT which are present at a

1:1 w/w ratio exist in dynamic equilibrium with bound hydrocarbon and SWNT. The data within this concentration range fits well to the solid lines which are a plot of Equation 4, resulting in a C_0 value of ~1.2 x 10^{-9} M for *p*-terphenyl in the presence of H-SWNT and ~3 x 10^{-9} M in the presence of AD-SWNT. The value indicates that below ~3 x 10^{-9} M for *p*-terphenyl the hydrocarbon molecules are interacting with SWNT where the surface area (bundle size) of the SWNT is constant. Deviation from the fit above ~4 x 10^{-8} M for *p*-terphenyl is attributed to an increase in the SWNT bundle surface area. [1,5] Within the concentration range of ~4 x 10^{-8} to ~1 x 10^{-5} M for *p*-terphenyl, isolated *p*-terphenyl molecules are interacting with SWNT of increasing surface area (bundle size). Above this concentration the fluorescence of the fraction of free *p*-terphenyl decreases due to the interaction between bundles of SWNT and aggregated *p*-terphenyl.

Comparing Figure 5 and 9 it is noted that after purification the fluorescence of *p*-terphenyl no longer exceeds 1.0 between a concentration range of 5 x 10^{-10} M to 4 x 10^{-8} M for AD-SWNT and 5 x 10^{-10} M to 5 x 10^{-6} M for H-SWNT respectively. This would indicate that the impurities with in the samples were responsible for the additional fluorescence observed. Exactly what in the impurities causes this effect is unknown and requires further studies, however the effect is no longer observed after purification. It is also noted that the degree of quenching (the extent of interaction between the SWNT and *p*-terphenyl) is similar for both AD-SWNT and H-SWNT in their purified state and this also holds true for the rate of bundle dispersion. The results indicate that in their purified state, replacing one SWNT type for another in the case of interaction with *p*-terphenyl has little bearing on the results obtained. However replacing one SWNT type with another in their as produced state will have bearing on the results obtained as it has been shown in the case of *p*-terphenyl that the hydrocarbon interacts not only with the SWNT but also the impurities in the sample therefore affecting the degree of interaction with the SWNT and the rate of bundle dispersion.

CONCLUSION

This paper investigated the interaction and bundle dispersion of SWNT produced by arc discharge and HiPco method in the presence of *p*-terphenyl in toluene. The study showed that under similar conditions that the degree of interaction of SWNT with *p*-terphenyl will vary in accordance with the amount of impurities present as the impurities interact with *p*-terphenyl and therefore hamper the hydrocarbon's interaction with SWNT and the rate of bundle dispersion. Once the SWNT samples were purified, however, the degree of interaction and the rate of bundle dispersion were similar. The studied also showed that while *p*-terphenyl will solubilise SWNT in toluene and disperse bundles it does not exclusively interact with SWNT in an untreated sample and therefore it is not an ideal molecule for processing an untreated sample of SWNT.

ACKNOWLEDGMENT. The AFM instrumentation used in this work was funded by the Science Foundation of Ireland (01/PI.2/C033).

REFERENCES.

(1) Hedderman, T.G.; Keogh, S.M.; Chambers, G.; Byrne H.J. *J. Phys. Chem. B.*, **2006**, 110, 3895

(2) Hedderman, T.G.; Keogh, S.M.; Chambers, G.; Byrne H.J. *J. Phys. Chem. B.*, **2004**, 108, 18860

(3) Dalton, A.; Stephan, C.; Coleman, J.N.; McCarthy, B.; Ajayan, P.M.; Lefrant, S.; Bernier, P.; Blau, W.J.; Byrne, H.J. *J. Phys. Chem. B.*, **2000**, 104, 10012.

(4) Dalton, A.; Blau, W.J.; Chambers, G.; Coleman, J.N.; Henderson, K.; Lefrant, S.; McCarthy, B.; Stephan, C.; Byrne, H.J. *Synth. Metals*, **2001**, 121, 1217.

(5) Coleman, J.N.; Maier, S.; Fleming, A.; O'Flaherty, S.; Minett, A.; Ferreira, M.S.; Hutzler, S.; Blau, W.J. *J. Phys. Chem. B.,* **2004**, 108, 3446.

(6) Giordani, S.; Bergin S.D.; Drury, A.; Mhuircheartaigh, E.; Ruther, M.; Coleman, J.N.; Blau, W.J. *Proceedings SPIE*, **2005,** 5842,. 42.

(7) Keogh, S.M.; Hedderman, T.G.; Gregan, E.; Farrell, G.; Chambers, G.; Byrne, H.J. *J. Phys. Chem. B.*, **2004**, 108, 6233

(8) Thess, A. ; Lee, R. ; Nikolaev, P. ; Dai, H. ; Petit, P. ; Robert, J. ; Xu, C. ; Lee, Y.H. ; Kim, S.G. ; Rinzler, A.G. ; Colbert, D.T. ; Scuseria, G.E. ; Tomanek, D. ; Fisher, J.E. ; Smalley, R.E. *Science,* **1996**, 273, 483.

(9) Nikolaev, P.; Bronikowski, M.J.; Kelley Bradley, R.; Rohmund, F.; Colbert D.T.; Smith, K.A.; Smalley, R.E. *Chem. Phys. Letts*., **1999**, 313, 91.

(10) Colomer, J.F.; Benoit, J.M.; Stephan, C.; Lefrant, S.; Van Tendeloo, G.; Nagy, J.B.; *Chem. Phys. Lett.,* **2001**, 345, 11.

(11) Bethune, D.S.; Kiang, C.H.; de Vries, M.S.; Gorman, G.; Savoy, R.; Vazquez, J.; Beyers, R. *Nature*, **1993**, 363, 605.

(12) Journet, C.; Bernier, P.; *Appl. Phys. A*., **1998**, 67, 1.

(13) Cheng, F.Li.; Xing, Y.T.; Tan, P.H.; Su, G.; *Carbon*, **2000**, 38, 2041.

(14) Bahr, J.L.; Mickelson, E.T.; Bronikowski, J.; Smalley, R.E.; Tour, J.M. *Chem. Comm*., **2001**, 193.

(15) Okahara, K.; Tanaka, K.; Aoki, H.; Sato, T.; Yamabe, T.; *Chem. Phys. Letts*.; **1994**, 19, 462.

(16) Ausman, K.D.; Piner, R.; Lourie, O.; Ruoff, R.S.; Korobov, M.; *J. Phys. Chem. B*., **2000**, 104, 8911.

(17) Cai, L.; Bahr, J.L.; Yao, Y.; Tour, J.M.; *Chem. Mater.* **2002**, 14, 4235.

(18) Chiang, I.W.; Brinson, B.E.; Huang, A.Y.; Willis, P.A.; Bronikowski, M.J.; Margrave, J.L.; Smalley, R.E.; Hauge, R.H.; *J. Phys. B.* **2001**, 105, 8297.

(19) Hagen, A.; Hertel, T.; *Nanoletters*, **2003**, 3, 383.

(20) Yu, Z.; Brus, L.; *J. Phys. Chem. B.*, **2001**, 105, 1123.

(21) Ryabenko, A.G.; Dorofeeva, T.V.; Zvereva, G.I., *Carbon*, **2004**, 42, 1523.

(22) Hamon, M.A.; Itkis, M.E.; Niyogi, S.; Alvaraez, T.; Kuper, C.; Menon, M.; *J. Am. Chem. Soc.*, **2001**, 123, 11292.

(23) Bachilo, S.M.; Strano, M.S.; Kittrell, C.; Hauge, R.H.; Smalley, R.E.; Weisman, R.B.; *Science*, **2002**, 298, 2361.

(24) Kataura, H.; Kumazawa, Y.; Maniwa, Y.; Umezu, I.; Suzuki, S.; Ohtsuka, Y.; Achiba, Y.; *Synthetic Metals*, **1999**, 103, 2555.

(25) Holden, J.M., Zhou, P., Bi, X., Eklund, P.C., Bandow, S., Jishi, R.A., Chowdhury, K.D., Dresselhaus, G., Dresselhaus, M.S., *Chem. Phys. Lett.*, **1994**, 220, 186.

(26) Journet, C., Maser, W.K., Bernier, P., Loiseau, A., Lamy de la Chapelle, M., Lefrant, S., Deniard, P., Lee, R., Fisher, J.E., *Nature*, **1997**, 388, 756.

(27) Alvarez, L., Righi, A., Rols, S., Anglaret, E., Sauvajol, A.L., *Amorphous and Nanostructures of Carbon,* **2000**, 53, 107, Material Research Society, Boston.

Available at: http://www.geocities.com/CollegePark/3972/MRS_99.pdf, accessed 26 March 2006.

(28) Socrates, G., *Infrared and Raman Characteristic Group Frequencies, Tables and Charts*, **2001,** John Wiley and Sons, Ltd., third edition, New York, 157-170.

(29) O'Connell M.J., Bachilo S.M., Huffman C.B., Moore V.C.; Strano M.S., Haroz E.H., Rialon, K.L., Boul P.J., Noon W.H., Kittrell C., Ma, J., Hauge, R.H., Weiseman R.B., Smalley R.E., *Science*, **2002**, 297, 593.

(30) Chakarova, S.; Schroder, E.; *J. Chem. Phys.*, **2005**, 122, 054102-1.

(31) Lee, N.K.; Kim, S.K.; *J. Chem. Phys*., **2005**, 122, 031102-1.

(32) Zacharia, R.; Ulbricht, H.; Hertel, T. *Phy. Rev. B*., **2004**, 69, 155406-1.

(33) Meehan, P.; Rayment, T.; Thomas, R.K. *J. Chem. Soc., Faraday I*, **1980,** 76, 2011.